Force/Velocity Manipulability Analysis for 3D Continuum Robots

Force/Velocity Manipulability Analysis for 3D Continuum Robots

Mohsen Khadem, Lyndon da Cruz, Christos Bergeles

Abstract—The enhanced dexterity and manipulability offered by continuum manipulators makes them the robot of choice for more complex procedures. However, many capabilities of continuum robots such as safe and effective manipulation will remain largely inaccessible without tailored analytical tools to evaluate their manipulability. This paper presents a quantifiable measure for analysing force/velocity manipulability of continuum robots. We expand classical measures of manipulability for rigid robots to introduce three types of manipulability indices as they apply to continuum robots, namely, velocity, compliance, and unified force-velocity manipulability. We provide a specific case study using the proposed method to analyse the force/velocity manipulability for a concentric-tube robot. We investigate the application of the manipulability measures to compare performance of continuum robots in terms off compliance and force/velocity manipulability. The proposed manipulability measures enables future research on design and optimal path planning for continuum robots.

I. INTRODUCTION

Continuum robots are continously flexible manipulators that can traverse confined spaces, manipulate objects in complex environments, and conform to curvilinear paths in space. Continuum robots have also made a significant impact in robotic surgery [1]–[4]. The enhanced dexterity and manipulability offered by continuum manipulators is an important factor enabling increasingly less invasive and more complex procedures. However, to the best of the authors' knowledge, established measure for quantifying manipulability of continuum robots does not exist. In this paper, we generalize classic manipulability analysis of rigid-link robots to introduce several measures that quantify a continuum robot's manipulability. The proposed measures can be used for analysis and comparison of designs of continuum robots. In addition, they allow the implementation of manipulability in optimal force/velocity motion planning for complex tasks.

A. Background

Manipulability describes the degree to which a manipulator can freely apply forces and torques or move in arbitrary directions, and quantifies the ability to perform an action quickly and skilfully [5], [6]. Manipulability analysis consists of describing directions in the task or joint space of a robot with the best ratio between some measure of effort in joint

space (e.g., joint torque) and a measure of performance in task space (e.g, position accuracy). Yoshikawa introduced the manipulability index [6] as a quality index for a single manipulator, which describes the characteristics of feasible motions in the task space corresponding to unit joint velocity vectors. He proposed a measure of manipulability based on analysis of the velocity manipulability ellipsoid (ME). Velocity ME is a volume/surface in the Cartesian velocity space, which is mapped from the unit sphere in the joint velocity space by a Jacobian transformation [6]. ME provides one of the standard tools for studying a manipulator's characteristics, and a large volume of work discussing rigid-link robot MEs exists.

Analogous to the velocity ellipsoid, researchers have defined a force ME for describing the force transmission characteristics of a manipulator at a given configuration. Considering the conservation of energy and viewing a robotic manipulator as a mechanical transformer, one can deduce that the principal axes of the velocity and force ellipsoids coincide, and the lengths of the axes are in inverse proportions [6], [7]. This means the optimal direction for effecting velocity (maximum velocity transmission ratio) is also the optimal direction for controlling force (minimum force transmission ratio). Similarly, the optimal direction for effecting force is also the optimal direction for controlling velocity.

Continuum robots have a fundamentally different structure than conventional rigid manipulators. Unlike rigid-link robots, where the pose of any point on the robot can be fully defined by link lengths and joint angles, the pose of a continuum robot is a function of the manipulator's shape and elasticity. Regardless of this significant difference between the rigid and continuum of manipulators, the models and mathematics derived for rigid robots can be generalized to include continuum robots. Gravagne *et al.* [8] proposed an approach to unify theories for force/velocity manipulability of rigid-link robots and continuum robots. They modelled a continuum robot as a serial robot with finite number of rigid links connected via revolute joints and expanded definitions of velocity/force MEs to introduce new types of MEs for continuum robots, namely, velocity and compliance ellipsoids. However, their approach was 2D and limited by modelling choices.

Recently several approaches have been proposed for estimating the velocity ME of continuum robots similar to rigid-link robots [9]. The resulting MEs can be employed to design optimal feasible paths for continuum robots [10]. Wu *et al.* introduced a kinematics-based dexterity index by comparing possible configurations when reaching a specific spatial position with area of a unit sphere placed around that position [11]. Konrad *et al.* used velocity manipulability index to design implicit active constraints for continuum robots [12]. The constraints were used to rapidly inform the operator with visual and haptic cues about the global and configuration-specific manoeuvrability of the robot. So far, The proposed

manipulability/dexterity measures only consider kinematics of the robot or solely rely on velocity ME. However, due to the inherent compliance and elasticity of continuum robots, the common force-velocity duality does not govern their motion, and the optimal direction for effecting force is not necessarily the optimal direction for controlling velocity. Thus, motion-planning based on velocity ME, can lead the robot to position and orientations, where it is incapable of applying any force.

The rest of the paper is organized as follows. In Section II, first, an overview of continuum robot kinematics is given. Next, the velocity and compliance manipulability ellipsoids for a continuum robot are presented. Finally, the compliance and velocity measures of robot manipulability are employed to develop a unified force-velocity manipulability for continuum robots that can estimate the optimal direction for effecting velocity and controlling force. Application of the proposed indices in investigating the manipulability of a concentric tube robots are studied in Section III. Concluding remarks appear in Section IV.

B. Contributions

The aim of this research is to develop manipulability indices for quantifying the dexterity of continuum robots. The proposed manipulability indices can be used in design and motion planning of continuum robots to enhance control over the force/velocity of robot end-effector, minimize the robot's footprint, optimize the control effort, and avoid singularities and joint limits of the robot. Also, manipulability indices can be employed as a measure of kinematic similarity in design of rigid-link master robots for master/slave teleoperated robotic systems that benefit from a continuum slave manipulator. We provide a specific case study, applying our framework to concentric tube robots [13], [14].

II. MANIPULABILITY OF CONTINUUM ROBOTS

In this section, several force/velocity measures for quantifying the manipulability of continuum robots are presented. We note that throughout this paper we use the following notation: x, $\boldsymbol{x}$ and $\mathbf{x}$ denote a scalar, a vector and a matrix, respectively. The prime and dot denote derivatives with respect to spatial coordinate s and time t.

A. Model of Continuum Robots

The kinematics of continuum robots can be decomposed into two mappings, a mapping between the robot's configuration space and task space, and a mapping between actuator space and configuration space [15]. We can write the model of a continuum robot with actuator values, $\boldsymbol{q}$ under 6 degrees of freedom (DoF) generalized forces $\boldsymbol{f}$ as follows

$$\boldsymbol{u}' = h(s, \boldsymbol{u}, \mathbf{g}, \boldsymbol{q}, \boldsymbol{f}), \tag{1a}$$

$$\mathbf{g}' = \mathbf{g}\hat{\epsilon}(\boldsymbol{u}), \tag{1b}$$

where $\boldsymbol{u}$ denotes the curvature and configuration of the robot backbone as a function of generalized forces $\boldsymbol{f}$ and actuators values $\boldsymbol{q}$, $\mathbf{g}(s) \in SE(3)$ is a homogeneous transformation defining the robot's backbone location and orientation in task space at arc length s. The superscript ^ denotes a skew

symmetric matrix under the mapping $\hat{\ } : \mathbb{R}^3 \to so(3)$, $\boldsymbol{\epsilon}$ is a body frame twist describing evolution of $\mathbf{g}$ as a function of $\boldsymbol{u}$. $\mathbf{g}(s)$ is defined as

$$\mathbf{g}(s) = \begin{bmatrix} \mathbf{R}(s) & \boldsymbol{r}(s) \\ \boldsymbol{0}^T & 1 \end{bmatrix}, \tag{2}$$

where $\boldsymbol{r}$ is the arc-length parametrized shape of the robot and $\mathbf{R} \in SO(3)$ is a rotation matrix at every arc-length location s on the robot.

B. Velocity Manipulability

In this section, we propose an approach for quantifying the manipulability of continuum robots using the model given in (1). First we define the Jacobian matrix for a continuum robot that maps the joint velocities ($\dot{\boldsymbol{q}}$) to the robot end-effector velocity ($\dot{\boldsymbol{x}}$). Based on (1), one can find the robot end-effector position-orientation $\boldsymbol{x}$ by solving

$$\dot{\boldsymbol{x}} = (\dot{\mathbf{g}}(\ell)\mathbf{g}^{-1}(\ell))^{\vee}, \tag{3}$$

where ℓ is the length of the robot.

Now, we can calculate the Jacobian for continuum robots through mechanics approximation as

$$\mathbf{J} = \frac{\Delta \boldsymbol{x}}{\Delta \boldsymbol{q}} = \begin{bmatrix} \dfrac{\boldsymbol{x}^T(\boldsymbol{q} + \frac{\Delta q_1}{2}\boldsymbol{e}_1) - \boldsymbol{x}^T(\boldsymbol{q} - \frac{\Delta q_1}{2}\boldsymbol{e}_1)}{\Delta q_1} \\ ... \\ \dfrac{\boldsymbol{x}^T(\boldsymbol{q} + \frac{\Delta q_n}{2}\boldsymbol{e}_n) - \boldsymbol{x}^T(\boldsymbol{q} - \frac{\Delta q_n}{2}\boldsymbol{e}_n)}{\Delta q_n} \end{bmatrix}^T \tag{4}$$

where $\boldsymbol{e}_i$ is the ith unit vector of the canonical basis of the n-dimensional joint space. $\mathbf{J}$ in (4) is the robot Jacobian, a mapping from $\boldsymbol{q} \in \mathbb{R}^n$ to $\boldsymbol{x} \in \mathbb{R}^6$. There are various methods for estimating the Jacobian [16]. We select the above formulation as it gives rise to parallelisable computations without sacrifices in the kinematics model's accuracy [10].

Extending the traditional definition of manipulability measure to continuum robots, we can define the velocity manipulability ellipsoid as

$$\text{VME} = \{\dot{\boldsymbol{x}} :\parallel \dot{\boldsymbol{q}} \parallel = 1\}. \tag{5}$$

VME is a mapping from a unit sphere in joint space to an ellipsoid in task space and describes the versatility of moving in the task space. The VME is a surface/volume that helps to visualize the feasible directions of velocity at the end-effector of a robot. The unit sphere in $\mathbb{R}^n$ can be mapped into $\mathbb{R}^6$ through $\mathbf{J}$ as shown bellow:

$$\|\dot{\boldsymbol{q}}\|^2 = \dot{\boldsymbol{q}}^T \dot{\boldsymbol{q}} = \dot{\boldsymbol{x}}^T (\mathbf{J}^{\dagger})^T (\mathbf{J}^{\dagger}) \dot{\boldsymbol{x}} = \dot{\boldsymbol{x}}^T (\mathbf{J}\mathbf{J}^T)^{-1} \cdot \dot{\boldsymbol{x}} \tag{6}$$

The superscript "$\dagger$" indicates the pseudo-inverse of a matrix, $\mathbf{J}^{\dagger} = \mathbf{J}^T (\mathbf{J}\mathbf{J}^T)^{-1}$.

Based on (6) the VME can be spanned using the singular values of the Jacobian matrix given by $J = U\Sigma V^T$, where $U = [u_1 \cdots u_6]$ is a unitary matrix, Σ is an $6 \times n$ rectangular diagonal matrix in which the diagonal entries ($\sigma_i, i = 1 \cdots 6$) are known as the singular values of J with $\sigma_1 \geq \sigma_2 \geq \cdots \geq \sigma_6$, and $V = [v_1^T \cdots v_n^T]$ is an $n \times n$ unitary matrix. The VME spanned by singular values of $\mathbf{J}$ has principal axis vectors $\boldsymbol{v}_i$ with magnitudes $\sqrt{\sigma_i}$, where $\boldsymbol{v}_i$ and $\sigma_1 \geq \sigma_2 \geq \cdots \geq \sigma_m$ are the eigenvectors and singular values of $\mathbf{J}$.

Now, the manipulability index μ can be defined proportional to the volume of the ME spanned by the singular values of J

$$\mu = \sqrt{det(\mathbf{J}\mathbf{J}^T)} = \sigma_1 \sigma_2 \cdots \sigma_6, \tag{7}$$

where μ is the manipulability index at a certain configuration in the robot's workspace.

In addition to the manipulability index, the isotropy of the robotic arm is also important [5]. It is a measure of how well the continuum robot can move in all directions, i.e., directional uniformity.The isotropy index has been introduced as the inverse of the condition number of the Jacobian

$$\frac{1}{\kappa} = \frac{1}{\|\mathbf{J}\|\|\mathbf{J}^{-1}\|} = \frac{\sigma_m}{\sigma_1}. \tag{8}$$

The manipulability μ and isotropy $1/\kappa$ indices can be used as a measure of kinematic dexterity of the continuum robot in free space.

C. Compliance Manipulability

The pose of a continuum robot is a function of the manipulator's elasticity. The inherent passive compliance of a continuum manipulator is very useful and can often eliminate the need for complex and expensive force/torque sensors and feedback systems. Passive compliance is also a practical and straightforward means to increase the safety margin of human robot interaction without relying on image/force feedback, which is useful for applications in surgical robotics [1]. In order to quantify the compliance of continuum manipulators, we introduce the compliance manipulability ellipsoid (CME) as

$$\text{CME} = \{\dot{\boldsymbol{x}} : \| \dot{\boldsymbol{f}} \| = 1\}. \tag{9}$$

The CME provides the critical first step in evaluating and effectively using a compliant system. Now using (1) and (3) we can calculate the compliance matrix for continuum robots through mechanics approximation as

$$\mathbf{C} = \frac{\Delta \boldsymbol{x}}{\Delta \boldsymbol{f}} = \begin{bmatrix} \dfrac{\boldsymbol{x}^T(\boldsymbol{f} + \frac{\Delta f_1}{2}\boldsymbol{e}_1) - \boldsymbol{x}^T(\boldsymbol{f} - \frac{\Delta f_1}{2}\boldsymbol{e}_1)}{\Delta f_1} \\ ... \\ \dfrac{\boldsymbol{x}^T(\boldsymbol{f} + \frac{\Delta f_6}{2}\boldsymbol{e}_6) - \boldsymbol{x}^T(\boldsymbol{f} - \frac{\Delta f_6}{2}\boldsymbol{e}_6)}{\Delta f_6} \end{bmatrix}^T, \tag{10}$$

where $\boldsymbol{e}_i$ is the ith unit vector of the canonical basis of the 6-dimensional generalized force space. $\mathbf{C}$ in (4) is the robot compliance matrix, a mapping from $\boldsymbol{f} \in \mathbb{R}^6$ to $\boldsymbol{x} \in \mathbb{R}^6$.

From (10), we can deduce $\|\dot{\boldsymbol{f}}\|^2 = \dot{\boldsymbol{x}}^T(\mathbf{C}\mathbf{C}^T)^{-1}\dot{\boldsymbol{x}}$. Thus, the CME can be spanned using the singular values of the Compliance matrix and has principal axis vectors $\boldsymbol{w}_i$ with magnitudes $\sqrt{\eta_i}$, where $\boldsymbol{w}_i$ and $\eta_1 \geq \eta_2 \geq \cdots \geq \eta_m$ are the singular values and eigenvalues of $\mathbf{C}$. The compliance manipulability index ν can be defined proportional to the volume of the CME

$$\nu = \eta_1 \eta_2 \cdots \eta_m. \tag{11}$$

Similar to velocity manipulability analysis, we can also define compliance isotropy index as in (8). In the next section, we use the velocity and compliance manipulability to define a unified force-velocity manipulability index for continuum robots.

D. Unified Force-Velocity Manipulability

For rigid-link robots the end-effector forces that a robot can produce given actuator torques of unit norm are estimated using the force manipulability ellipsoid

$$\text{FME} = \{\boldsymbol{f} : \| \boldsymbol{\tau} \| = 1\}, \tag{12}$$

where $\boldsymbol{\tau}$ is the robot joint torques.

In rigid-link robots, end-effector forces are related to joint torques using the transpose of Jacobian. Thus, the force ME has principal axis vectors $\boldsymbol{v}_i$ with magnitudes $1/\sqrt{\sigma_i}$ and is perpendicular to the velocity ME. This indicates that the directions in which the robot can exert the greatest forces are also the directions in which it is least sensitive to changes in the actuator displacements. However, unlike with rigid-link robots, the torques felt at the actuators of a continuum robot do not necessarily reflect the end-effector generalized forces and include the elastic energy of the robot backbone. Even in the absence of gravity and when the robot is not moving, joint torques are required to hold the manipulator in a given pose. Thus, the VME cannot be directly related to FME, and is only applicable when the robot is in free space or the external forces are negligible.

We propose an approach to unify the force and velocity manipulability ellipsoids for continuum robots. We introduce a new measure of manipulability that considers the inherent compliance of the continuum robot, and can be used to estimate optimal direction for applying velocity and force when the robot end-effector is under external forces, i.e, interacting with an object. First, assuming the robot is in a static equilibrium, the principle of virtual work dictates

$$\boldsymbol{\tau}^T \delta \boldsymbol{q} = \boldsymbol{f}^T \delta \boldsymbol{x} + \int_0^{\ell} \boldsymbol{u}^T \mathbf{K} \delta \boldsymbol{u} \mathrm{d}s, \tag{13}$$

where $\mathbf{K}$ is the robot's stiffness matrix. The first term in (13) corresponds to the work done by robot actuators, the second term is the work done by robot at its end-effector, and finally the third term is due to the elastic energy stored in the robot backbone as it deforms. From (10), it is evident that a force contour corresponding to a constant change in distributed joint torque $\boldsymbol{\tau}$ will not be elliptical in general, and the classical velocity-force duality cannot be employed to estimate robot force manipulability.

To overcome this problem, we start with a simple two-step thought experiment. First, assuming that the robot is relatively rigid, i.e., $\delta \boldsymbol{u} \simeq 0$, the continuum robot behaves similar to a rigid-link robot. It acts as a mechanical transformer of velocities and forces from the joint space to the task space. Second, assuming that the robot joints are fixed under external forces, i.e., $\delta \boldsymbol{q} \simeq 0$, the robot behaves similar to a compliant passive manipulator and the external work of applied forces are stored as the strain energy of the robot backbone. This prompts the observation that the continuum manipulator under external forces at its end-effector behaves similar to a dual-arm robotic system comprised of a rigid-link manipulator and a passive compliant manipulator.

Here, we employ approach that is common in manipulability analysis of multiple cooperating robots [17], [18] to develop a quantifiable measure of manipulability of continuum robots, which accounts for passive compliant of the robot. Motivated by the above discussion, we follow the approach

first presented in [19] to simulate the motion of the robot end-effector as a dual-arm robotic system comprised of a rigid-link manipulator and a passive compliant manipulator, manipulating a mass-less point object with tight grasps. The rigid manipulator transforms the joint velocities/torques to end-effector velocity/force using the VME defined in (5). The passive compliant manipulator restricts the motion of the rigid robot via dissipating the rigid robot energy. Considering the two end-effectors are connected, the motion of the passive manipulator can be investigated using the CME defined in (5).

First we introduce the unified manipulability ellipsoid as

$$\text{FME} = \{\dot{\boldsymbol{x}} : \parallel \dot{\boldsymbol{q}} \parallel = 1 \; \& \; \Lambda = \text{const.}\}, \quad (14)$$

where Λ is the desired stiffness at the robot end-effector. In the first step, it is assumed that the rigid robot acts as a mechanical transformer, thus, the motion of the robot end-effector is given using the Jacobian as $\dot{x} = \dot{q}$. In the next step, considering that the robot joints remain constant, i.e., $\dot{q} = 0$, the interaction force between the robot and the environment, $\boldsymbol{h}$, pushes the compliant manipulator in the opposite direction by magnitude of $\boldsymbol{x} = \mathbf{C}\boldsymbol{h}$. Finally, considering that the desired stiffness of the manipulator end-effector is Λ, the interaction force between the robot and the environment at the equilibrium can be obtained as

$$\boldsymbol{f} = \Lambda \mathbf{C} \boldsymbol{h} \quad (15)$$

Note that using our discretized approximation we have considered the effect of the energy stored in the robot backbone. Now, using the principle of virtual work we have

$$\boldsymbol{\tau}^T \delta \boldsymbol{q} = \boldsymbol{f}^T \delta \boldsymbol{x}. \quad (16)$$

Replacing $\delta \boldsymbol{x}$ and $\boldsymbol{f}$ using (4) and (15) we obtain

$$\boldsymbol{\tau} = \mathbf{J}^T \mathbf{C} \Lambda \boldsymbol{h} \quad (17)$$

At this point, wthe pre-image of the unit sphere in the extended joint torque space under the mapping (17) is given by $\boldsymbol{h}^T [\mathbf{J}^T \mathbf{C} \Lambda \Lambda^T \mathbf{C}^T \mathbf{J}] \boldsymbol{h}$.

Now based on the force-velocity duality, the unit sphere in the joint velocity space $\dot{\boldsymbol{q}}$ maps into

$$\dot{\boldsymbol{x}}^T [\mathbf{J}^T \mathbf{C} \Lambda \Lambda^T \mathbf{C}^T \mathbf{J}]^{-1} \dot{\boldsymbol{x}}, \quad (18)$$

which is defined as the UME ellipsoid and can by a set of principal axes $\lambda_i \boldsymbol{z}_i$ where λ_i and $\boldsymbol{z}_i$ are the singular values and eigen vectors of matrix $\Lambda^T \mathbf{C}^T \mathbf{J}$. In Section III, we evaluate the accuracy of the proposed manipulability in predicting optimal direction robot end-effector in contact with an environment.

E. Manipulability Constraints

For continuum robots, beside the singular values and manipulability index, joint limits have a major impact on the robot end-effector dexterity in the workspace. In order to consider the effects these constraints, we employ constrained Jacobian $\mathbf{J}^c$ and Compliance $\mathbf{C}^c$. The constrained Jacobian and compliance are formed by penalizing the columns of the matrices individually using

$$\mathbf{J}_i^c = P_i^c \mathbf{J}_i, \; \mathbf{C}_i^c = P_i^c \mathbf{C}_i \quad (19)$$

where J_i is the ith column of the robot Jacobian. P_i^c is the joint-wise penalization function given by

$$P_i^c = \frac{1 - exp(\frac{-4k_c(q_i - q_{i,min})(q_{i,max} - q_i)}{(q_{i,max} - q_{i,min})^2})}{1 - exp(-k_c)} \quad (20)$$

where the coefficient "4" and the denominator "$1 - exp(-k_c)$" in equation (19) are needed to normalize the penalization term such that P_i^c spans the interval $[0,1]$. At the joint-limits, P_i^c becomes zero. In the neutral position, P_i^c becomes one. The scaling coefficient k_c specifies the functional shape in between these points. Using this penalty function, the individual columns of $\mathbf{J}$ and $\mathbf{C}$ are penalized when the ith joint value q_i approaches the limits $q_{i,min}$ or $q_{i,max}$. This penalization approach has been used to contraint robot jacobian in [9], [20]. Now, by substituting the constrained Jacobian $\mathbf{J}^c$ and compliance matrix $\mathbf{C}^c$ in (4) and (10), we can calculate the VME, CME, and UME considering the robot mechanical constraints.

III. Case Study:Manipulability Analysis of Concentric Tube Robots

In this section, we apply the methods derived above to analyse the manipulability of a concentric-tube robot. Concentric tube robots are composed of series of precurved elastic tubes that can be axially translated and rotated with respect to each other to control the shape of the robot (see Fig. 1) [13], [14]. Here, we give a brief summary of that model before applying the methods of Section II.

A. Concentric Tube Robot Model

In this section, a 3D model of a concentric tube robot is presented. The model for the statics of concentric tube robots have been derived in [14], [21]. Each tube of the robot is modelled as a deformable curve endowed with triad of vectors forming a frame attached to every point. By convention, the frame is chosen so that the z-axis of $\mathbf{R}$ remains tangent to the curve. The configuration of each tube of the robot can be uniquely defined using a unique line of centroids, $\boldsymbol{r}(s) : [0, \ell] \to \mathbb{R}^3$, and a unique family of orthogonal transformations, $\mathbf{R}(s) : [0, \ell] \to SO(3)$. The differential kinematic equations describing the evolution of the transformation are given as $\mathbf{g}' = \mathbf{g}\hat{\boldsymbol{\epsilon}}$, where $\boldsymbol{\epsilon} = [\boldsymbol{e}_3 \; \boldsymbol{u}^T]^T$, and $\boldsymbol{e}_3 = [0, \; 0, \; 1]^T$. $\boldsymbol{u}(s)$ is the curvature of tube and is given by

$$\boldsymbol{u}(s) = (\dot{\mathbf{R}}\mathbf{R}^{-1})^\vee, \quad (21)$$

Considering the tubes are made of linear elastic isotropic materials and following the approach discussed in [13], [14], we can derive the constitutive equation for calculating the instantaneous curvature of tubes. First, we break the robot into several segments between transitions points, at which the continuity of shape and internal moment must be enforced (see Fig. 1). Each segment can contain 1 to i tubes. Next, we consider that the final deformed curve of all tubes at a given time t must be equal to the curve of the most inner tube $^i\boldsymbol{r}(s,t) = {}^1\boldsymbol{r}(s,t)$. To parametrize the tubes twist, we assume the rotation matrix of the tubes are different from the most inner tube by one rotation about axial unit vector, i.e., $^i\mathbf{R}(s,t) = {}^1\mathbf{R}(s,t)\mathbf{R}_{i\boldsymbol{\theta}}(s,t)$. Finally, based on these assumptions the curvature of tubes can be calculated using Euler's laws of Balance of momentum and moment of momentum as follows

$$^i\boldsymbol{r}'(s,t) = {}^i\mathbf{R}(s,t)\boldsymbol{e}_3, \quad (22a)$$

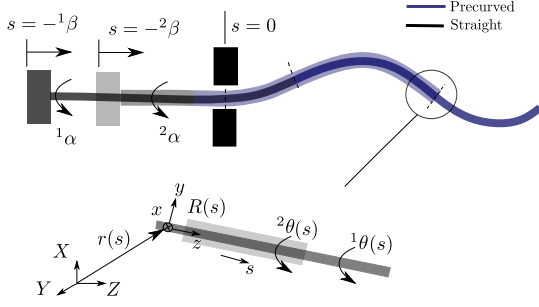$$^i\mathbf{R}'(s,t) = {}^i\mathbf{R}(s,t)^i\hat{\mathbf{u}}(s,t), \quad (22b)$$

Fig. 1. A schematic of a concentric tube robot. Tubes are grasped at their respective proximal ends, and the actuation variables i^α and i^β denote the proximal base rotation and translation, respectively. Each tube is comprised of a straight and a curved section. i^θ denotes angular displacement of tube i.

$$
\begin{aligned}
{}^1u'_n = &-\left(\sum_{i=1}^{N} {}^i\mathbf{K}^{-1}\right)\sum_{i=1}^{N}\mathbf{R}_{\mathrm{i}\boldsymbol{\theta}}\left[{}^i\mathbf{K}\left({}^i\theta'\frac{\mathrm{d}\mathbf{R}_{\mathrm{i}\boldsymbol{\theta}}}{\mathrm{d}^i\theta}{}^1\boldsymbol{u} - {}^i\boldsymbol{U}'\right)\right.\\
&\left.+ {}^i\hat{\mathbf{u}}{}^i\mathbf{K}\left({}^i\boldsymbol{u}-{}^i\boldsymbol{U}\right)\right]\\
&-\left(\sum_{i=1}^{N}{}^i\mathbf{K}^{-1}\right)\left[\boldsymbol{e}_3\times{}^1\mathbf{R}^T\int_s\boldsymbol{f}(\epsilon,t)\mathrm{d}\epsilon\right]\Bigg|_n, \quad n=1,2 ,
\end{aligned}
$$
$$\tag{22c}$$

$$
{}^iu'_3 = {}^iU'_3 + \frac{{}^iE^iI}{{}^iG^iJ}(u^i{}_1{}^iU_2 - {}^iu_2{}^iU_1), \tag{22d}
$$

$$
{}^iu'_n = \mathbf{R}_{\mathrm{i}\boldsymbol{\theta}}{}^1\boldsymbol{u} + {}^i\theta'\boldsymbol{e}_3\Big|_n, \quad n=1,2, \tag{22e}
$$

where, superscript i $(i=1,...,N)$ denote the parameters and variables of the ith tube and subscripts n $(n=1,2,3)$ denote the nth element of a vector. $\boldsymbol{U}^i$ is the curvature of each tube in its reference configuration. Also, $\theta'^i = u_3^i - u_3^1$ denotes the angle of twist about z-axis with respect to the most inner tube, and ${}^i\mathbf{K} = \mathrm{diag}({}^iE^iI, {}^iE^iI, {}^iG^iJ)$. E is the Young's modulus, I is the second moment of inertia, G is the shear modulus, and J is the polar moment of inertia of tube. $\boldsymbol{f}$ is the external force applied to the robot.

The initial conditions can be specified in terms of these unknown quantities and the actuator values as follows

$$
\boldsymbol{r}(0) = [0\ 0\ 0]^T, \tag{23a}
$$

$$
\mathbf{R}(0) = \begin{bmatrix} cos({}^1\alpha + {}^1\beta^1 u_3) & -sin({}^1\alpha + {}^1\beta^1 u_3) & 0 \\ sin({}^1\alpha + {}^1\beta^1 u_3) & cos({}^1\alpha + {}^1\beta^1 u_3) & 0 \\ 0 & 0 & 1 \end{bmatrix},
$$
$$\tag{23b}$$

$$
\theta^i(0) = ({}^i\alpha + {}^i\beta^1 u_3) - ({}^1\alpha + {}^1\beta^1 u_3), \tag{23c}
$$

where the actuator value vector $\boldsymbol{q}$ consists of the rotations and translations of each tube, ${}^i\alpha$ and ${}^i\beta$, shown in Fig. 1. (22) and (23) can be solved to estimate robot backbone curvature and robot end-effector position and orientation, $\mathbf{g}(\ell)$.

B. Simulation Study

We now provide simulation results using the discussed model for a concentric-tube robot with two tubes. The mechanical properties of the tubes are given in Table I.

In the first simulation we examined the accuracy of velocity manipulability ellipsoid in predicting the direction of motion of the robot end-effector. Representative results are shown in Fig. 2. The robot motion with respect to unit change in

TABLE I
PHYSICAL PARAMETERS FOR TUBES USED IN SIMULATIONS.

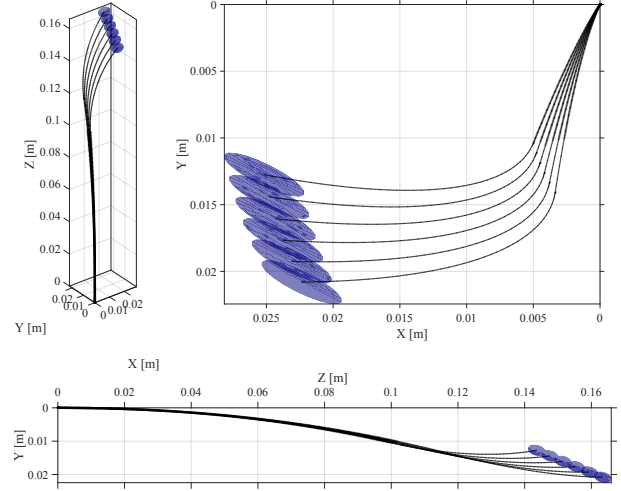|	Tube 1	Tube 2
Inner Diameter [mm]	1	1.75
Outer Diameter [mm]	1.5	2.5
Straight Length [mm]	15	10
Curved Length [mm]	35	15
Curvature [m^{-1}]	15	7.5
Young's Modulus, E [GPa]	30	30
Shear Modulus, G [GPa]	11	11

Fig. 2. An illustration of the VME (blue ellipse) for a concentric tube robot.

joint variables $\boldsymbol{q}$, as well as the VMEs are plotted. The initial configuration of the robot is ${}^1\alpha = 0$, ${}^2\alpha = \frac{\pi}{2}$, ${}^1\beta = 40$[mm], ${}^2\beta = 10$[mm]. The velocity manipulability is shown in blue. For visualization, we only plotted the 3D ellipsoid regarding the translational motion of the robot end-effector. As it can be seen in Fig. 2, the VME can estimate the optimal direction of motion with respect to a unit change in joint variables and provides a measure of effort in joint space and robot motion in task space.

In the next simulation, we studied the accuracy of compliance ellipsoid. The CME can estimate the direction of motion of robot end-effector with respect to a unit change in generalized forces in task space. Figs. 3 illustrate the nature of the compliance ellipsoid. The the initial configuration of the robot is ${}^1\alpha = 0$, ${}^2\alpha = \frac{\pi}{2}$, ${}^1\beta = 35$[mm], ${}^2\beta = 5$[mm]. In each figure, the concentric tube robot starts in the same no-load configuration, and then experiences three equal end-effector forces increasing from 0 to 10 N, applied separately in x, y, and z directions on local frame of the robot end-effector. A force applied in the positive y direction (Fig. 3(b)), produce a much greater end-effector displacement than when applied in local x and z directions (Fig. 3(a) and 3(c)). As it can be seen, the ellipsoid gives excellent insight into the relative response of the backbone of the concentric tube robot in each case.

As discussed in Section II-C, the inherent compliance of a continuum manipulator can be used to increase safety of robotic manipulation. In the next simulation, we studied the variations in CME and robot compliance as a function of robot pose and configuration. The robot compliant can be used
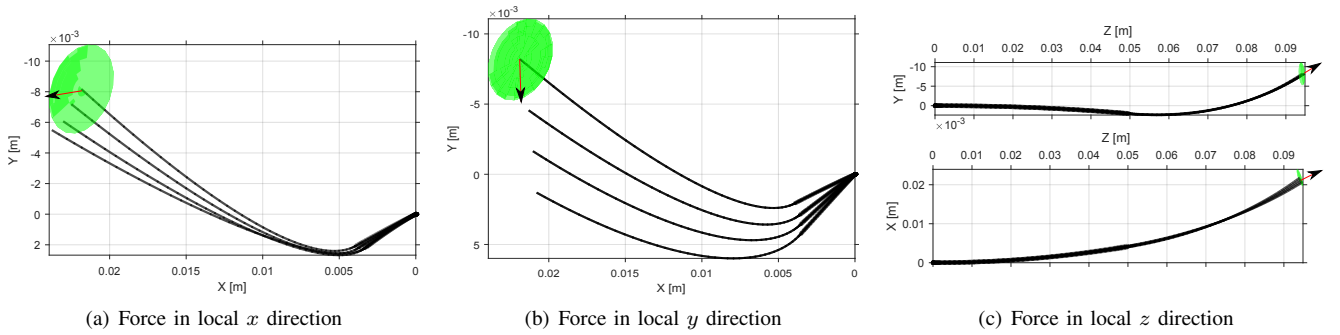
(a) Force in local x direction

(b) Force in local y direction

(c) Force in local z direction

Fig. 3. Simulation results for robot under forces of the same magnitude at x, y, and z directions on local frame of the robot end-effector. Forces are shown with red arrows. CME is scaled down by a factor of 0.1
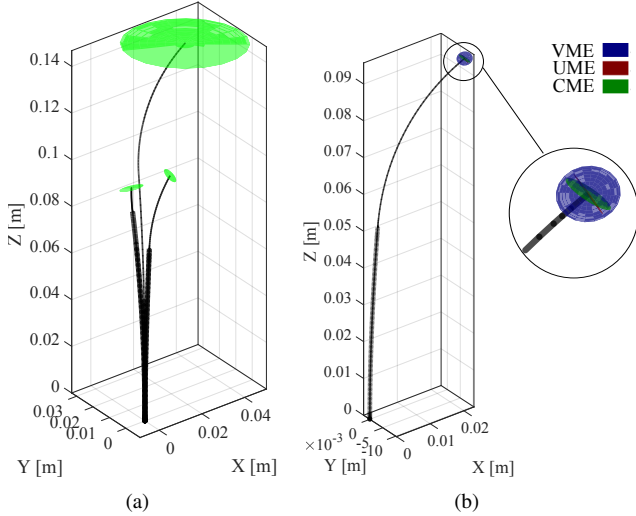

(a)

(b)

Fig. 4. (a) Effect of moving the robot outer tube and shape of the robot backbone on direction, orientation and volume of robot CME. CMEs are scaled down a factor of 0.5. (b) A schematic of a concentric tube robot and the velocity, compliance, and unified force-velocity manipulability ellipsoids.

to increase the safety of robot interaction with soft tissue in surgical robots. As it can be seen in Fig. 4(a), by changing the length of the robot tubes, i.e., $^1\beta$ and $^2\beta$, we can control the shape and direction of CME. Thus, CME can be used to study robot compliance throughout its workspace.

In the next simulation, the application of unified force-velocity manipulability ellipsoid (UME) in quantifying the robot interactions are studied. The velocity, compliance, and unified force-velocity manipulability ellipsoids for a specific configuration of the robot are shown in Fig. 4(b). As mentioned before, the VME only considers kinematics of the continuum robot in free space. However, because of the compliance of continuum robots backbone the optimal direction for effecting force is not necessarily the same as VME. This fact can be seen in Fig. 4(b), as the direction of optimal velocities when the robot is in contact with an object (shown in red) is very different from optimal velocity direction shown by VME (in blue).

Figs. 5 illustrate the accuracy of UME in estimating the the optimal direction of motion with respect to a unit change in joint variables, when the robot is in contact with an object. In the simulations, the desired stiffness of the robot end-effector Λ is 1 N/mm in all directions, i.e, $diag(1\cdots1)$. In each figure, the concentric tube robot starts in the same no-

load configuration in contact with a rigid object, and then start moving in response to unit change in joint variables $^1\beta$ (Fig. 5(a)) and $^1\beta$ (Fig. 5(b)), i.e, change in 1st and 2nd tube length. For comparison, results of robot motion when it is in free space is plotted in blue. Based on the results, when the robot moves the greatest motion is in local y direction as the UME shown in red predicts. Also, the robot is almost incapable of moving in z direction as the UME has the smallest value in that direction.

Unlike VME, the UME gives excellent insight into the concentric tube robot motion in contact when it is applying force. This can be clearly seen in bottom figure in Fig. 5(a). When the robot moves in free space it can freely extend toward z direction. However, when it is in contact with an object, because of the backbone compliance, it is forced to move along y direction. Revisiting the duality between velocity and force again, it can be found that an optimal direction to actuate a velocity is also an optimal direction to control a force. Thus, for the continuum robot in the given configuration, in terms of end-effector velocity, the performance is better along the local y axis while in terms of end-effector forces, higher forces can be applied along z direction.

IV. CONCLUDING REMARKS

The enhanced dexterity and manipulability offered by continuum robots such as the concentric tube robot can significantly improve the performance of minimally invasive surgeries. In this paper, we proposed several manipulability indices to quantify the manipulability of continuum robots, namely, velocity, compliance, and unified force-velocity manipulability. First, by generalizing the previous manipulability measures commonly employed in manipulability analysis of rigid robots, we introduced a velocity manipulability index which describes the feasible motions of continuum robot end-effector in the Cartesian space corresponding to unit joint velocity vectors. We showed that due to inherent compliance of a continuum robot, a velocity ME cannot predict optimal directions for applying force when the robot is in contact with the environment. Next, we proposed a compliance manipulability to quantify the compliance of the continuum manipulator. Finally, we employed the compliance and velocity manipulability to introduce a unified force-velocity manipulability measure. The unified force-velocity ME can be conveniently utilized not only for analysing manipulability of the continuum robot along different directions of the operational space, but also
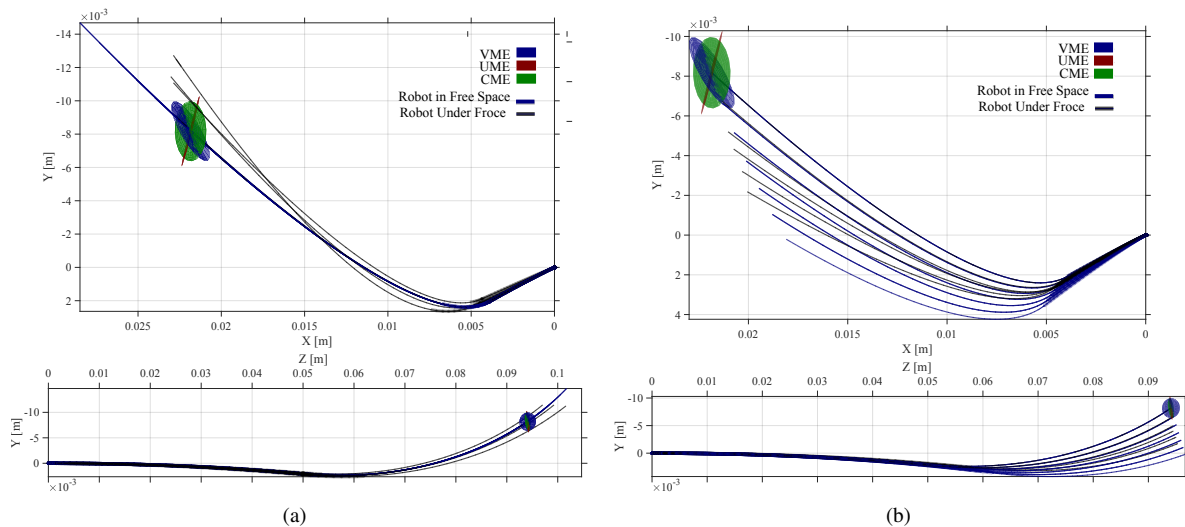
Fig. 5. Result simulation for a robot connected to a spring. Velocity, Compliance, and Unified force-velocity manipulability ellipsoids are shown. (a) Robot motion in response to unit change in inner tube length $^1\beta$ (b) Robot motion in response to unit change in outer tube length $^2\beta$)

for determining compatibility of the structure to execute a task assigned along a direction. Several simulations were performed to validate the proposed manipulability analysis.

In future, we will use the proposed measures of manipulability in design and control of concentric tube robots. Such a quantifiable measure of dexterity can be used for analysis and comparison of designs of concentric tube robots. Also, the proposed analysis allows for considering dexterity in motion scaling, motion planning, and control of complex surgical tasks such as suturing or navigation in the presence of anatomical obstacles.

REFERENCES

[1] J. Burgner-Kahrs, D. C. Rucker, and H. Choset, "Continuum robots for medical applications: A survey," *IEEE Transactions on Robotics*, vol. 31, no. 6, pp. 1261–1280, Dec 2015.

[2] H. B. Gilbert, J. Neimat, and R. J. Webster, "Concentric tube robots as steerable needles: Achieving follow-the-leader deployment," *IEEE Transactions on Robotics*, vol. 31, no. 2, pp. 246–258, 2015.

[3] C. Bergeles, A. H. Gosline, N. V. Vasilyev, P. J. Codd, P. J. del Nido, and P. E. Dupont, "Concentric tube robot design and optimization based on task and anatomical constraints," *IEEE Transactions on Robotics*, vol. 31, no. 1, pp. 67–84, 2015.

[4] J. Burgner, D. C. Rucker, H. B. Gilbert, P. J. Swaney, P. T. Russell, K. D. Weaver, and R. J. Webster, "A telerobotic system for transnasal surgery," *IEEE/ASME Transactions on Mechatronics*, vol. 19, no. 3, pp. 996–1006, 2014.

[5] J. K. Salisbury and J. J. Craig, "Articulated Hands: Force Control and Kinematic Issues," *The International Journal of Robotics Research*, vol. 1, no. 1, pp. 4–17, 1982.

[6] T. Yoshikawa, "Manipulability of Robotic Mechanisms," *The International Journal of Robotics Research*, vol. 4, no. 2, pp. 3–9, 1985.

[7] S. L. Chiu, "Task compatibility of manipulator postures," *The International Journal of Robotics Research*, vol. 7, no. 5, pp. 13–21, 1988.

[8] I. A. Gravagne and I. D. Walker, "Manipulability, force, and compliance analysis for planar continuum manipulators," *IEEE Transactions on Robotics and Automation*, vol. 18, no. 3, pp. 263–273, 2002.

[9] K. Leibrandt, C. Bergeles, and G. Z. Yang, "On-line collision-free inverse kinematics with frictional active constraints for effective control of unstable concentric tube robots," in *2015 IEEE/RSJ International Conference on Intelligent Robots and Systems (IROS)*, 2015, pp. 3797–3804.

[10] ——, "Implicit active constraints for safe and effective guidance of unstable concentric tube robots," in *2016 IEEE/RSJ International Conference on Intelligent Robots and Systems (IROS)*, 2016, pp. 1157–1163.

[11] L. Wu, R. Crawford, and J. Roberts, "Dexterity analysis of three 6-dof continuum robots combining concentric tube mechanisms and cable-driven mechanisms," *IEEE Robotics and Automation Letters*, vol. 2, no. 2, pp. 514–521, 2017.

[12] K. Leibrandt, C. Bergeles, and G. Z. Yang, "Implicit active constraints for concentric tube robots based on analysis of the safe and dexterous workspace," in *2017 IEEE/RSJ International Conference on Intelligent Robots and Systems (IROS)*, 2017, pp. 193–200.

[13] R. J. Webster, J. M. Romano, and N. J. Cowan, "Mechanics of precurved-tube continuum robots," *IEEE Transactions on Robotics*, vol. 25, no. 1, pp. 67–78, 2009.

[14] P. E. Dupont, J. Lock, B. Itkowitz, and E. Butler, "Design and control of concentric-tube robots," *IEEE Transactions on Robotics*, vol. 26, no. 2, pp. 209–225, 2010.

[15] D. C. Rucker and R. J. W. III, "Statics and dynamics of continuum robots with general tendon routing and external loading," *IEEE Transactions on Robotics*, vol. 27, no. 6, pp. 1033–1044, 2011.

[16] D. C. Rucker and R. J. Webster, "Computing jacobians and compliance matrices for externally loaded continuum robots," in *2011 IEEE International Conference on Robotics and Automation*, 2011, pp. 945–950.

[17] A. Bicchi, C. Melchiorri, and D. Balluchi, "On the mobility and manipulability of general multiple limb robots," *IEEE Transactions on Robotics and Automation*, vol. 11, no. 2, pp. 215–228, 1995.

[18] C. Melchiorri, "Multiple whole-limb manipulation: An analysis in the force domain," *Robotics and Autonomous Systems*, vol. 20, no. 1, pp. 15 – 38, 1997.

[19] P. Chiacchio, S. Chiaverini, L. Sciavicco, and B. Siciliano, "Global task space manipulability ellipsoids for multiple-arm systems," *IEEE Transactions on Robotics and Automation*, vol. 7, no. 5, pp. 678–685, 1991.

[20] P. Wisanuvej, G. Gras, K. Leibrandt, P. Giataganas, C. A. Seneci, J. Liu, and G.-z. Yang, "Master Manipulator Designed for Highly Articulated Robotic Instruments in Single Access Surgery," in *IEEE/RSJ International Conference on Intelligent Robots and Systems (IROS)*, 2017.

[21] D. C. Rucker, B. A. Jones, and R. J. W. III, "A geometrically exact model for externally loaded concentric-tube continuum robots," *IEEE Transactions on Robotics*, vol. 26, no. 5, pp. 769–780, 2010.